Wear 268 (2010) 443–454

Contents lists available at ScienceDirect

Wear

journal homepage: www.elsevier.com/locate/wear

The elastic–plastic indentation response of a columnar thermal barrier coating

Th. Zisis*, N.A. Fleck

Department of Engineering, University of Cambridge, Cambridge CB2 1PZ, UK

ARTICLE INFO

Article history:
Received 28 November 2008
Received in revised form 3 August 2009
Accepted 25 August 2009
Available online 1 September 2009

Keywords:
Thermal barrier coatings
Indentation
Fracture

ABSTRACT

Thermal barrier coatings with a columnar microstructure are prone to erosion damage by a mechanism of surface cracking upon impact by small foreign particles. In order to explore this erosion mechanism, the elastic indentation and the elastic–plastic indentation responses of a columnar thermal barrier coating to a spherical indenter were determined by the finite element method and by analytical models. It was shown that the indentation response is intermediate between that of a homogeneous half-space and that given by an elastic–plastic mattress model (with the columns behaving as independent non-linear springs). The sensitivity of the indentation behaviour to geometry and to the material parameters was explored: the diameter of the columns, the gap width between columns, the coefficient of Coulomb friction between columns and the layer height of the thermal barrier coating. The calculations revealed that the level of induced tensile stress is sufficient to lead to cracking of the columns at a depth of about the column radius. It was also demonstrated that the underlying soft bond coat can undergo plastic indentation when the coating comprises parallel columns, but this is less likely for the more realistic case of a random arrangement of tapered columns.

© 2009 Elsevier B.V. All rights reserved.

1. Introduction

Thermal barrier coatings (TBCs) are used in gas turbines in order to allow for an increased operating temperature and thereby to increased thermodynamic efficiency. In broad terms, a top layer of zirconia provides the thermal barrier, a much thinner intermediate layer of alumina provides the environmental barrier and a bottom layer of highly alloyed nickel bonds the alumina layer to the nickel-based superalloy substrate [1]. The top layer is termed the *thermal barrier layer*, the alumina layer is the *thermally grown oxide* (TGO) *layer* and the bottom layer of aluminium-rich nickel alloy is the *bond coat* (BC).

The top thermal barrier layer commonly comprises yttria stabilised zirconia (YSZ), and in gas turbine coatings for aerospace application this layer is deposited as a columnar microstructure by electron beam, physical vapour deposition (EB-PVD). The layer is of thickness 100–200 μm and each column is an epitaxially grown single crystal of diameter about 10 μm. A gap of width 0.1–1 μm exists between each column and provides *strain tolerance* to the coating. These gaps open and close in order to accommodate the thermal strain mismatch associated with the temperature gradients and the temperature transients of normal engine operation.

The service life of the columnar layer is often dictated by particle erosion: the erosive particles can be small worn fragments from the upstream combustor or, in the case of an aircraft engine, they can be ingested into the gas turbine. The initial impact response, on a time scale of nanoseconds, is elasto-dynamic, and is dealt with in a separate publication [2]. After the initial elasto-dynamic phase, the particles slow down and the subsequent response is quasi-static. At small indent depths the imposed strain level is low while the imposed strain rate is high: this results in an elastic quasi-static indentation response. Subsequently, a larger indent may develop and plastic deformation occurs at the top of the columnar microstructure. The main objective of the present paper is to assess the *elastic* indentation response and the *elastic–plastic* indentation response of the columnar thermal barrier coating by a rigid sphere. The sensitivity of the indentation response to the material properties of the multi-layer coating, to the geometry of the columns and to the level of friction between the columns were each explored by the finite element method. Analytical formulae were obtained for the contact size and for the indentation load by curve-fitting to the finite element results. The stress state within the columns adjacent to the contact was determined, and the likelihood of erosion was assessed for fracture from pre-existing edge defects within the columns. It is appreciated that this initial scoping investigation was somewhat idealised: in reality, particles impinge the TBC at an inclination to the TBC surface, and the incoming particles are angular in shape. Nonetheless, the analysis provides useful insight into the significance of the columnar microstructure on the indentation and erosion resistance of thermal barrier coatings. The

* Corresponding author. Present address: Department of Civil Engineering, University of Thessaly, Pedion Areos, 38334 Volos, Greece. Tel.: +30 242 1074179; fax: +30 242 1074169.
E-mail address: zisis@metal.ntua.gr (Th. Zisis).

0043-1648/$ – see front matter © 2009 Elsevier B.V. All rights reserved.
doi:10.1016/j.wear.2009.08.035

Nomenclature

Latin symbols

b	contact radius (μm)
$\bar{b}$	dimensionless contact radius
C	constraint factor
D	radius of spherical indenter (μm)
g	intercolumnar gap thickness (μm)
d	columnar thickness (μm)
E_{TBC}	Young's modulus of the thermal barrier coating (GPa)
H_{BC}	thickness of the bond coat layer (μm)
H_{TBC}	thickness of the thermal barrier coating layer (μm)
H_{TGO}	thickness of the thermally grown oxide layer (μm)
P	contact force (N)
$\bar{P}$	dimensionless contact force
p	contact pressure (GPa)
p_{av}	average contact pressure (GPa)
$\bar{p}$	dimensionless average contact pressure
r	radial distance form the centre line (μm)
R	radius of the spherical indenter (μm)
u	axial displacement of a point at the contact surface (μm)

Greek symbols

α	geometric constant depending on the degree of pile-up or sink-in
δ	indentation depth of the spherical indenter (μm)
σ_Y	yield strength (MPa)
σ_{TBC}	yield strength of thermal barrier coating (MPa)
σ_{TGO}	yield strength of thermally grown oxide (MPa)
σ_{BC}	yield strength of bond coat (MPa)
μ_c	intercolumnar Coulomb friction coefficient
μ_s	Coulomb friction coefficient between the surface of the indenter and the surface of the thermal barrier coating layer

problem of foreign object damage (FOD) will be dealt with in a separate publication; FOD entails gross deformation of the thermal barrier system, with the formation of a crater and the bending and cracking of a number of columns by a single impact.

Our study builds upon the preliminary analyses of Chen et al. [3]. They conducted a limited set of finite element simulations of the indentation of a columnar TBC coating by a spherical indenter. They showed that the indentation pressure increases with decreasing gap width between columns and with increasing intercolumnar friction coefficient. They did not separate though the elastic indentation response from the elastic–plastic response, and they did not make comparisons between numerical simulations and simple analytical formulae. Our intention in the present study is to present a more comprehensive treatment of the problem and to derive useful analytical approximations of the response.

1.1. Experimental evidence for erosion damage

Experimental evidence on engine hardware during accelerated high temperature testing or during service operation confirms that particles with a high kinetic energy cause the TBC to be susceptible to large plastic deformation and densification around the contact site. A range of plastic deformation patterns have been observed and the most representative types are now reviewed. In Fig. 1(a), plastic deformation at small indentation depths is observed. Plastic densification of the columns is evident, but cracking is absent at the boundaries of the columns. At high temperature (in excess of 800 °C) and at larger indentation depths, plastic bending of the columns is observed (Fig. 1(b)) but in this case no plastic densification and no cracking is evident [4]. A third deformation mechanism occurs at large indentation depths. Cross-sectioned samples of 7YSZ deformed at 1150 °C are shown in Fig. 1(c) and (d) [5,6]. Inside a densified zone, kink bands form and extend diagonally downward, toward the interface with the thermally grown oxide (TGO). Inside the bands, plastic bending of the columns is observed. Note that cracking can be observed at the boundaries of the kink band, thereby weakening the material. Similar responses have been observed during quasi-static indentation at elevated temperatures [3,5]. The similarity in response under impact and slow indentation conditions indicates that the qualitative features of the plasticity-based mechanisms governing material removal are not strongly affected by strain rate.

2. Analytical models for the elastic and plastic indentation response

We begin our study by reviewing idealised models for frictionless, spherical indentation of a columnar layer. It is anticipated that the indentation response of the columnar TBC system will be intermediate between that of a Winkler foundation of independent springs and that of a homogeneous half-space. First, the *elastic* indentation response of the TBC multi-layer is idealised by that of an elastic 'mattress' of springs upon a rigid substrate and by that of an elastic, homogeneous half-space (the Hertz solution). Second, the *elastic–plastic* indentation response of the TBC system is idealised by that of a rigid, ideally plastic mattress model and by that of a rigid, ideally plastic homogeneous half-space.

2.1. Elastic response: the mattress model

The columnar nature of the microstructure of the TBC layer suggests that the TBC can be modelled as a simple Winkler elastic foundation (i.e. an elastic mattress) rather than an elastic half-space [7]. The elastic foundation comprises springs in order to mimic the response of the columnar TBC layer of height H_{TBC}, and axial modulus E_{TBC}. The mattress rests upon a rigid base and is indented by a rigid, frictionless spherical indenter of radius R. At a representative instant in time, the TBC layer has been indented to a depth δ, with a contact radius b. The mattress model attempts to capture the normal indentation response when the columns behave independently and do not contact each other. It is anticipated that this idealisation is accurate in the regime where the TBC columns behave independently and the diameter of the TBC columns is much less than the radius of contact between spherical indenter and the TBC.

Upon compressing the coating, the contact pressure p, depends only on the vertical displacement at that point [7], thus

$$p = E_{TBC}\frac{u}{H_{TBC}} \tag{1}$$

where u is the vertical displacement of a point at the contact interface between the layer and the indenter, at a radial distance r from the centre line (see Fig. 2). Now consider indentation of the coating to a depth δ by a sphere of diameter D. The axial displacement u at a radius r from the central axis is

$$u = \delta - \frac{r^2}{D} \tag{2}$$

and the net contact force P is

$$P = \int_{r=0}^{b} [2\pi r p(r)]dr = \frac{2\pi E_{TBC}}{H}\left[\frac{\delta b^2}{2} - \frac{b^4}{4D}\right] \tag{3}$$

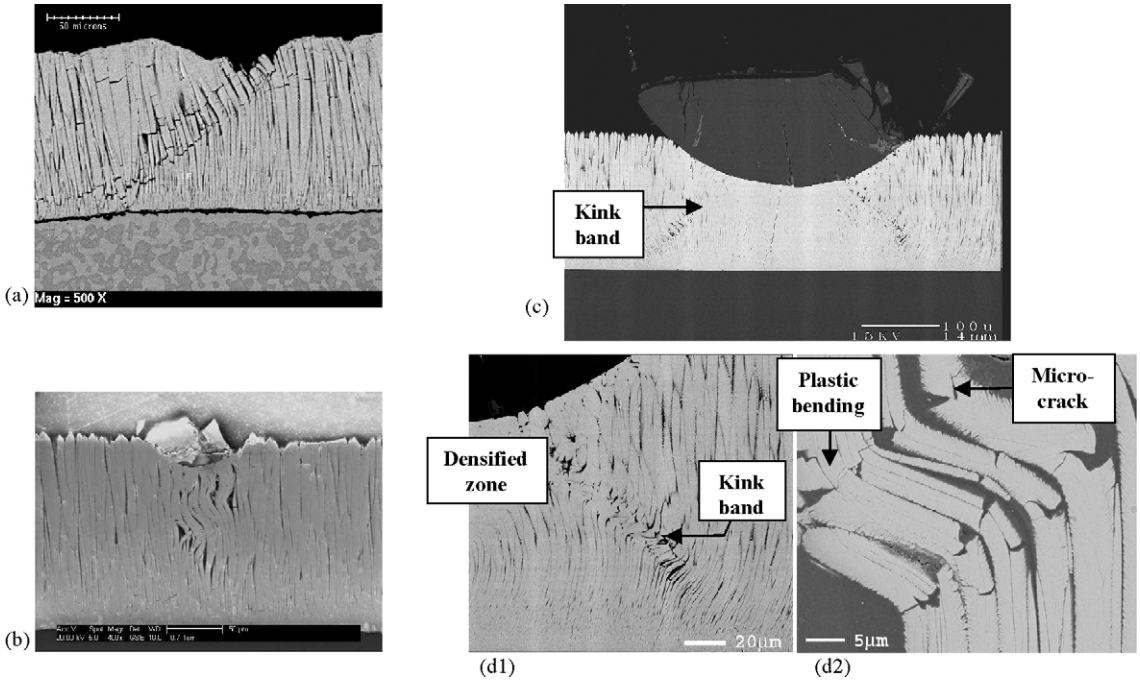

Fig. 1. (a) Cross-section of thermal barrier coating that has experienced near surface cracking under operating conditions (Courtesy of A.G. Evans). (b) Cross-section of eroded sample of TBC showing plastic deformation of the TBC at 800 °C [4]. (c) and (d) Scanning electron microscope images of cross-sections of a 7YSZ subjected to plastic penetration at 1150 °C [6].

Upon neglecting the presence of pile-up or sink-in at the edge of the contact, the contact radius b is

$$b^2 = D\delta \tag{4}$$

according to the intersecting chords theorem. Consequently, the indentation load is

$$P = \frac{\pi E_{\mathrm{TBC}} b^2 \delta}{2H_{\mathrm{TBC}}} = \frac{\pi E_{\mathrm{TBC}} D\delta^2}{2H_{\mathrm{TBC}}} \tag{5}$$

and the average pressure is $p_{\mathrm{av}} = P/\pi b^2 = P/\pi D\delta$ is

$$p_{\mathrm{av}} = \frac{E_{\mathrm{TBC}}\delta}{2H_{\mathrm{TBC}}} \tag{6}$$

It is useful to re-write the above analytical solution in non-dimensional form. The dimensionless contact radius is

$$\bar{b} \equiv \frac{b}{R} = \sqrt{2}\left(\frac{\delta}{R}\right)^{1/2} \tag{7}$$

and the dimensionless indentation load is

$$\bar{P} \equiv \frac{P}{R^2 E_{\mathrm{TBC}}} = \pi \frac{H_{\mathrm{TBC}}}{R}\left(\frac{\delta}{H_{\mathrm{TBC}}}\right)^2 \tag{8}$$

The non-dimensional average contact pressure p_{av} reads

$$\bar{p} \equiv \frac{p_{\mathrm{av}}}{E_{\mathrm{TBC}}} = \frac{1}{2}\left(\frac{\delta}{H_{\mathrm{TBC}}}\right) \tag{9}$$

2.2. The Hertz elastic solution

For comparison purposes, it is useful to quote the Hertz solution for indentation of an isotropic elastic half-space by a rigid, frictionless sphere [7]. The non-dimensional contact radius, load and average pressure are

$$\bar{b} \equiv \frac{b}{R} = \left(\frac{\delta}{R}\right)^{1/2}, \tag{10}$$

$$\bar{P} \equiv \frac{P}{E_{\mathrm{TBC}} R^2} = \frac{4}{3(1-\nu^2)}\left(\frac{H_{\mathrm{TBC}}}{R}\right)^{3/2}\left(\frac{\delta}{H_{\mathrm{TBC}}}\right)^{3/2} \tag{11}$$

and

$$\bar{p} \equiv \frac{p_{\mathrm{av}}}{E_{\mathrm{TBC}}} = \frac{4}{3\pi(1-\nu^2)}\left(\frac{H_{\mathrm{TBC}}}{R}\right)^{1/2}\left(\frac{\delta}{H_{\mathrm{TBC}}}\right)^{1/2}, \tag{12}$$

respectively.

The essential difference between the mattress model and the Hertz solution is that the indentation load is sensitive to layer height for the mattress model while it is independent of the layer height for the Hertz solution. Note that the power law dependence of load upon indent depth is also different for the two models.

2.3. Indentation of a rigid, ideally plastic half-space

The TBC coating is at a sufficiently high operating temperature for it to undergo power law creep at low strain rate and for it to undergo rate-independent plastic glide at high strain rates. Deformation mechanism maps have been constructed for polycrystalline zirconia to summarise this behaviour [8]. In this scoping study, we have assumed that the TBC layer behaves in an elastic-ideally plastic manner: this is the limiting case of negligible strain hardening and negligible strain rate hardening. A full analysis would include both strain hardening and strain rate sensitivity, with an evolution of the constitutive law from rate insensitive dislocation glide at high stresses to power law creep at intermediate stresses and thence to diffusional flow at low stress levels. The main thrust of the present work was to explore the sensitivity of the indentation response to the details of the columnar structure of the TBC layer, including the role of intercolumnar friction. The full indentation

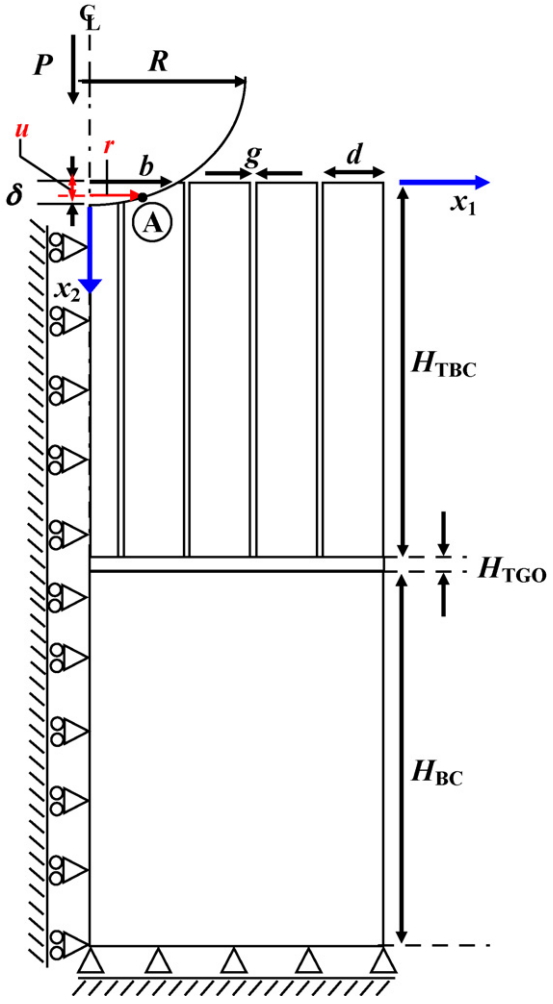

Fig. 2. Sketch of the quasi-static normal indentation of a thermal barrier system by a rigid sphere. The columnar thermal barrier coating (TBC) is adhered to an underlying thermally grown oxide (TGO) and bond coat. At A, a point of the contact interface between the indenter and the TBC layer, has a radial distance r from the centre line and an axial displacement u.

problem contains many intrinsic length scales and other parameters, and so extreme forms of the constitutive law were used in this exploratory study.

At sufficiently large indentation depths the TBC layer yields plastically. An approximate analytical model for the indentation response by a rigid, frictionless sphere can be obtained by assuming that the TBC layer behaves as a rigid, ideally plastic solid. First, we treat the TBC layer as a homogeneous half-space, and second as a mattress of independent columns. The contact radius b is related to the indentation depth δ by

$$b^2 = 2\alpha R\delta \tag{13}$$

where the geometric constant α depends upon the degree of pile-up or sink-in at the contact periphery. For a homogeneous half-space we have $\alpha = 1.44$ [9], while for mattress model we have $\alpha = 1.0$. In dimensionless form the contact radius reads

$$\bar{b} \equiv \frac{b}{R} = \sqrt{2\alpha}\sqrt{\frac{H_{\mathrm{TBC}}}{R}}\left(\frac{\delta}{H_{\mathrm{TBC}}}\right)^{1/2} \tag{14}$$

The indentation load P is related to the contact radius b by

$$P = C\sigma_{\mathrm{Y}}\pi b^2, \tag{15}$$

Table 1
Geometry of the thermal barrier system.

TBC thickness	50–200 μm
TBC column diameter	10–40 μm
TBC gap width	0.001–1 μm
TGO thickness	5 μm
Bond coat thickness	200 μm

where σ_{Y} is the yield strength, and the constraint factor C equals 3 for the homogeneous half-space while C equals unity for the mattress model. The indentation load P varies with indentation depth δ according to

$$P = 2C\alpha\sigma_{\mathrm{Y}}\pi R\delta \tag{16}$$

and in non-dimensional form this may be re-written as

$$\hat{P} \equiv \frac{P}{\sigma_{\mathrm{Y}}R^2} = 2C\alpha\pi\frac{H_{\mathrm{TBC}}}{R}\left(\frac{\delta}{H_{\mathrm{TBC}}}\right) \tag{17}$$

The non-dimensional average indentation pressure p_{av} is

$$\hat{p} \equiv \frac{p_{\mathrm{av}}}{\sigma_{\mathrm{Y}}} = C \tag{18}$$

3. Finite element study of the elastic indentation response of the thermal barrier coating system

It is instructive to compare the above analytical models with the more accurate finite element simulations of the indentation response.

3.1. Geometry and material properties

The finite element model used to simulate the elastic–plastic indentation of the TBC system by a sphere is sketched in Fig. 2. The columnar microstructure was adhered to a thin layer of thermally grown oxide (TGO) and, in turn, to the bond coat and underlying rigid substrate. The TBC layer had a height H_{TBC} with discrete columns of diameter d and intercolumnar gaps of width g. The opposing faces of the columns can slide with a Coulomb friction coefficient μ_{c}. Preliminary finite element simulations revealed that the level of friction between the top of the TBC layer and the spherical indenter are of minor importance. (The details of these calculations are not reported here for the sake of brevity.) Thus, all simulations presented here assume frictionless contact between the indenter and the TBC layer, unless otherwise stated. The TGO and bond coat have a height of H_{TGO} and H_{BC}, respectively. The range of assumed values for the geometry of the TBC system and the diameter D of the spherical indenter are listed in Table 1. Unless otherwise stated we assumed that $d = 10$ μm, $R = 100$ μm and $H_{\mathrm{TBC}} = 200$ μm.

The material properties of each layer are summarised in Table 2. In the first set of calculations each layer was treated as elastic. Then, in a second set of calculations, each layer was taken as elastic, ideally plastic. The assumed values of yield strength for the TBC layer were consistent with elevated temperature measurements conducted on single crystals of 10YSZ in the ⟨1 0 0⟩ orientation representative of the texture developed deposition [10].

Table 2
The elastic–plastic properties of the layers.

Material properties	Young's modulus E (GPa)	Poisson ratio ν	Yield strength at high temperature σ (MPa)
TBC	140		400/no yield
TGO	370/rigid	0.3	300/no yield
Bond coat	210/rigid		20/no yield

3.2. Finite element model

The commercial finite element program ABAQUS Standard [11] was employed for the numerical calculations. In order to perform a tractable finite element analysis, an axisymmetric model was constructed, with the columnar microstructure represented by annular array of circular cylinders with wall width d and intervening gap g. A cylindrical co-ordinate system was adopted, with x_1 as the radial co-ordinate and x_2 as the axial co-ordinate, see Fig. 2. The bottom of the bond coat was adhered to a rigid substrate (the nickel-based superalloy). A mesh sensitivity study revealed that adequate accuracy was achieved using about 210,000 four-noded quadrilateral axisymmetric elements, with reduced integration (CAX4R in ABAQUS notation). The nodal spacing in the contact zone was $0.002R$. The rigid contact surface option was employed to mimic the rigid spherical indenter. The side face of the axisymmetric mesh was taken to be traction free: numerical experimentation showed that the precise mesh boundary condition on the outer radius was unimportant when the mesh extends beyond about $5R$. Finite deformation effects were included by using the non-linear geometry option within ABAQUS Standard.

In the following sections, we examine the effect of the TBC geometry upon the contact radius, the indentation load, the average indentation pressure and the bending stresses within each column. First, we assume an elastic response and then we consider the elastic–plastic behaviour.

4. Finite element results for elastic indentation

The sensitivity of the elastic response to various material and geometric parameters is now reported. The main variables are the gap width, layer height of the TBC and the intercolumnar friction coefficient μ_c. Two sets of elastic calculation were performed: in the first set, the columnar thermal barrier layer, the TGO layer and the bond coat each deform elastically, using the values of Young's modulus quoted in Table 1. Then, in a second set of calculations, the columnar thermal barrier layer deforms elastically while the underlying TGO and bond coat were idealised as rigid.

4.1. Sensitivity of elastic indentation response to the gap width

The dimensionless contact radius, average pressure and indentation force are plotted as a function of dimensionless indentation depth in Fig. 3 for selected values of gap width g. The columns were taken to be frictionless, $\mu_c = 0$, and the gap width was taken to be $g = 0.01$, 0.1, and 1 μm. The height of the TBC layer was $H_{TBC} = 200$ μm and the radius of the sphere was $R = 100$ μm. Results are shown both for a rigid bond coat and for an elastic bond coat, and analytical solutions according to the Hertz solution and mattress model are included.

In each numerical simulation the sphere progressively contacted five annuli of columns with increasing indentation depth. The transition in contact radius b from one column to the neighbouring one resulted in a step-wise increase in the contact radius b/R (Fig. 3(a)). Between these transitions from one column to the next, the contact radius shows a small progressive increase with increasing indentation depth δ/R. The dimensionless gap width g/d (and the finite stiffness of the TGO and bond coat) have only a minor effect upon the contact radius, and the contact radius lies between the prediction (7) of the mattress model and the prediction (14) of the Hertz solution.

The evolution of average pressure p_{av} with indent depth δ is shown in Fig. 3(b). For clarity of presentation, only a fraction of the data points are shown explicitly, with the smooth curves giving the detailed trajectory of intermediate data points. A smaller gap

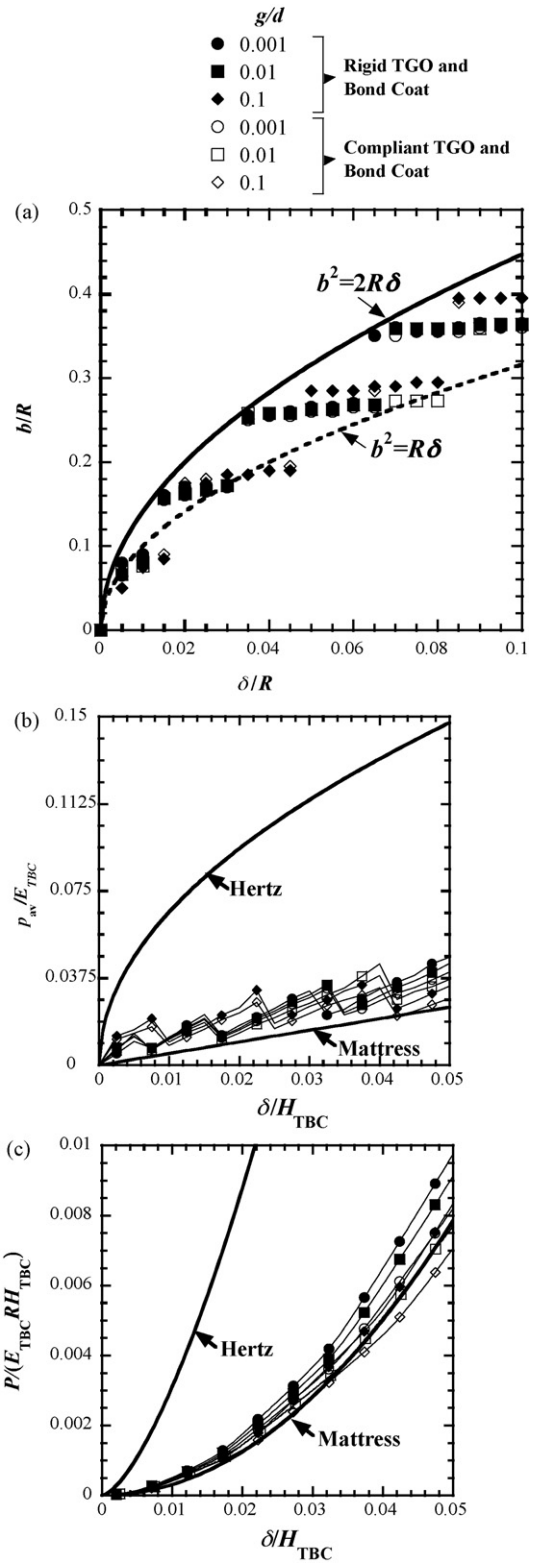

Fig. 3. (a) Contact radius (b) average indentation pressure and (c) indentation load as a function of the normalised indentation depth. The effect of the gap width g is shown for a columnar TBC resting on a compliant TGO and bond coat (with properties stated in Table 2), and for a columnar TBC resting on a rigid substrate. $R = 100$ μm, $H_{TBC} = 200$ μm, $d = 10$ μm, $\mu_c = \mu_s = 0$.

width leads to a slightly higher average contact pressure. Note that the compliance of the TGO and bond coat has a negligible effect upon p_{av}: the pressure on a TBC layer with a rigid underlying TGO and bond coat are slightly above those for a TBC system with a compliant TGO and bond coat.

The dimensionless indentation load $P/(E_{TBC}RH_{TBC})$ versus indentation depth δ/H_{TBC} is given in Fig. 3(c). The indentation load increases slightly with decreasing gap size g, and also increases upon making rigid the TGO and bond coat. The analytical responses, as given by the mattress model (8) and by Hertz solution (12), are included in Fig. 3: the numerical predictions suggest that the mattress model is more accurate than the Hertz solution for the columnar microstructure.

4.2. Sensitivity of elastic indentation response to the level of intercolumnar friction

Fig. 4 presents the effect of the intercolumnar Coulomb friction coefficient μ_c upon the dimensionless contact radius, average pressure and indentation load. Two choices of gap width were assumed: $g = 0.01$ μm and $g = 0.1$ μm. The height of the layer was $H_{TBC} = 200$ μm and the radius of the sphere was $R = 100$ μm. Again we took the TGO and bond coat system to be either rigid or compliant (using the moduli quoted in Table 2). It is clear from Fig. 4(a–c) that the magnitude of intercolumnar Coulomb friction coefficient μ_c and the stiffness of the substrate have only a minor effect upon the contact radius. The average pressure and the indentation load increase with decreasing gap width and with increasing intercolumnar Coulomb friction coefficient while the compliance of the TGO/TBC system is of minor importance.

The mattress model adequately predicts the response of the layer upon a rigid or frictionless substrate provided the intercolumnar contacts are frictionless. However, it does not account for the stiffer response with increasing intercolumnar friction and decreasing gap width. Finite element predictions with high intercolumnar friction and a vanishing gap width converge to the Hertz solution.

The presence of discrete columns has a major influence upon the contact stress field. This is illustrated by contours of axial stress σ_{22} in Fig. 5(a) for a columnar microstructure (frictionless columns with a gap width of $g = 0.1$ μm) and in Fig. 5(b) for a homogeneous layer. Both layers were indented to a depth of $\delta/H_{TBC} = 0.05$, and rest upon the compliant substrate. It is noted that the axial stress field is almost uniform within each column of the TBC layer (Fig. 5(a)), in support of the mattress model.

4.3. Sensitivity of elastic indentation response to the TBC layer thickness

The effect of the height of the thermal barrier coating layer upon the contact radius, average pressure and indentation load is summarised in Fig. 6(a), (b) and (c), respectively. The gap width was held fixed at $g = 0.1$ μm and all contacts were assumed to be frictionless. The height of the layer was assumed to be $H_{TBC} = 50$ and 200 μm, with the radius of the indenter R equaled to 100 μm and the column diameter d equaled to 10 μm. Accordingly, the ratio H_{TBC}/R equaled 0.5 and 2. Again, results are presented both for a rigid and a compliant substrate.

It is concluded from Fig. 6(a) that the type of the TGO/bond coat substrate (whether rigid or compliant) and the magnitude of the TBC layer height (over the range considered) have a negligible effect upon the contact radius: the contact radius is adequately approximated by the mattress model prediction (7). The mattress model also gives an adequate prediction (9) for the average indentation pressure p_{av} and (8) for the indentation load P: it is able to capture the effect of layer height H_{TBC} upon the contact stiffness. In contrast, the Hertz prediction is too stiff.

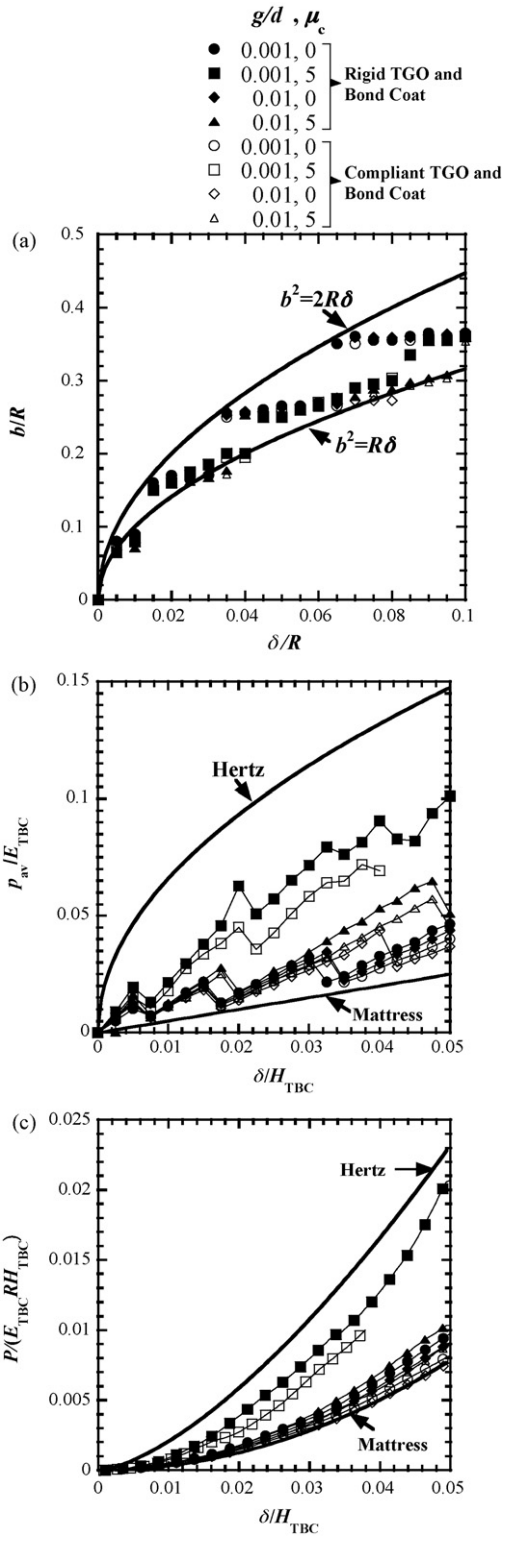

Fig. 4. (a) Contact radius (b) average pressure and (c) indentation load as a function of normalised indentation depth. The effect of the intercolumnar friction μ_c is shown for rigid and compliant substrates. $R = 100$ μm, $H_{TBC} = 200$ μm, $d = 10$ μm, $g = 0.1$ and 0.01 μm, $\mu_s = 0$.

4.4. Sensitivity of elastic indentation response to the diameter of the TBC columns

Fig. 7 presents the effect of column diameter d upon the contact radius b, the average pressure p and the indentation load P.

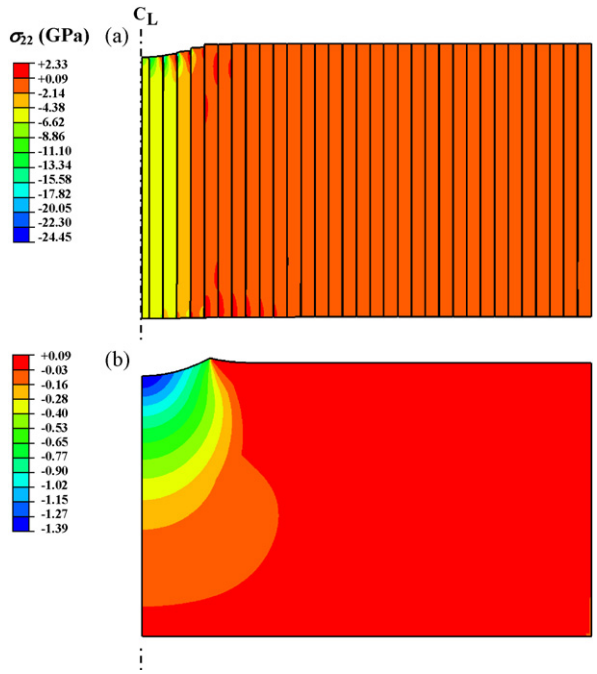

Fig. 5. Contours of stress component σ_{22} in (a) TBC columnar structure ($g/d = 0.1$, $\mu_c = 0$) and (b) homogeneous, isotropic TBC layer at $\delta/H_{TBC} = 0.05$. Both layers rest on a compliant TGO/bond coat substrate. Frictionless spherical indenter of radius $R = 100\,\mu m$, column diameter $d = 10\,\mu m$.

For this set of simulations the radius of the sphere is $R = 100\,\mu m$ and the column diameter was $d = 10$, 20 and 40 μm. The gap width g was 0.1 μm and all contacts were taken to be frictionless. Furthermore, the height of the TBC layer was $H_{TBC} = 200\,\mu m$. Taken together, the plots given in Fig. 7 show that the mattress model becomes increasingly accurate with decreasing d. At the opposite extreme of $d/D \to \infty$ the columnar structure behaves as a homogeneous elastic half-space and the Hertz solution will be recovered. As already noted in previous figures, the magnitude of the compliance of the substrate has a minor effect upon the response.

4.5. The propensity for fracture near the top of the columns

Recent work by Zisis and Fleck [2] has highlighted the development of high axial tensile stresses near the top of a columnar TBC coating under elasto-dynamic loading. These stresses are experienced on a nanosecond timescale after impact by the erosive particle, and they can lead to columnar fracture and removal. Write V as the particle velocity, E_{TBC} as the axial modulus of the TBC and ρ_{TBC} as the density. Then, the tensile stress has a peak value on the order of $V\sqrt{E_{TBC}\rho_{TBC}}$. Upon assuming $V = 300\,ms^{-1}$, $E_{TBC} = 140$ GPa, and $\rho_{TBC} = 5900\,kg\,m^{-3}$, the peak elasto-dynamic stresses are of order $0.06E_{TBC} = 8.6$ GPa. It is instructive to explore the evolution of axial stresses within the TBC layer under quasi-static elastic indentation, and to compare their magnitude with the levels encountered in the initial elasto-dynamic phase.

Representative results are reported here for the tensile axial stress within the columns during quasi-static elastic indentation. The TBC layer comprises frictionless columns of height $H_{TBC} = 200\,\mu m$, diameter $d = 10\,\mu m$ and gap width $g = 0.1\,\mu m$, indented by a sphere of radius $R = 100\,\mu m$. The peak algebraic values of axial stress σ_{22} within the 5 columns adjacent to the centre line are plotted as a function of the indentation depth δ in Fig. 8(a), while the distribution of tensile axial stress throughout the microstructure is plotted in Fig. 8(b) at $\delta/H_{TBC} = 0.05$. It is evident from Fig. 8(b) that the tensile stress peaks at the lateral

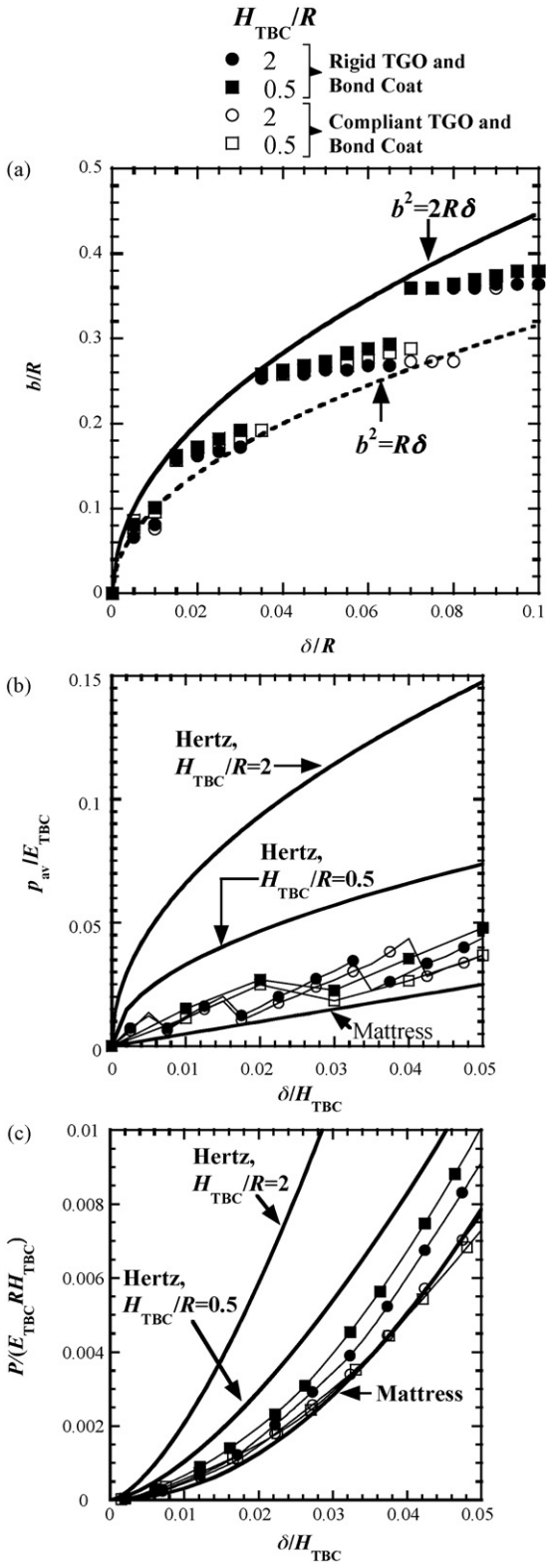

Fig. 6. (a) Contact radius (b) average pressure and (c) indentation load as a function of normalised indentation depth. The effect of the thickness H_{TBC} of the TBC layer is shown for rigid and compliant TGO/bond coat substrates. $R = 100\,\mu m$, $d = 10\,\mu m$, $g = 0.1\,\mu m$, $\mu_c = \mu_s = 0$.

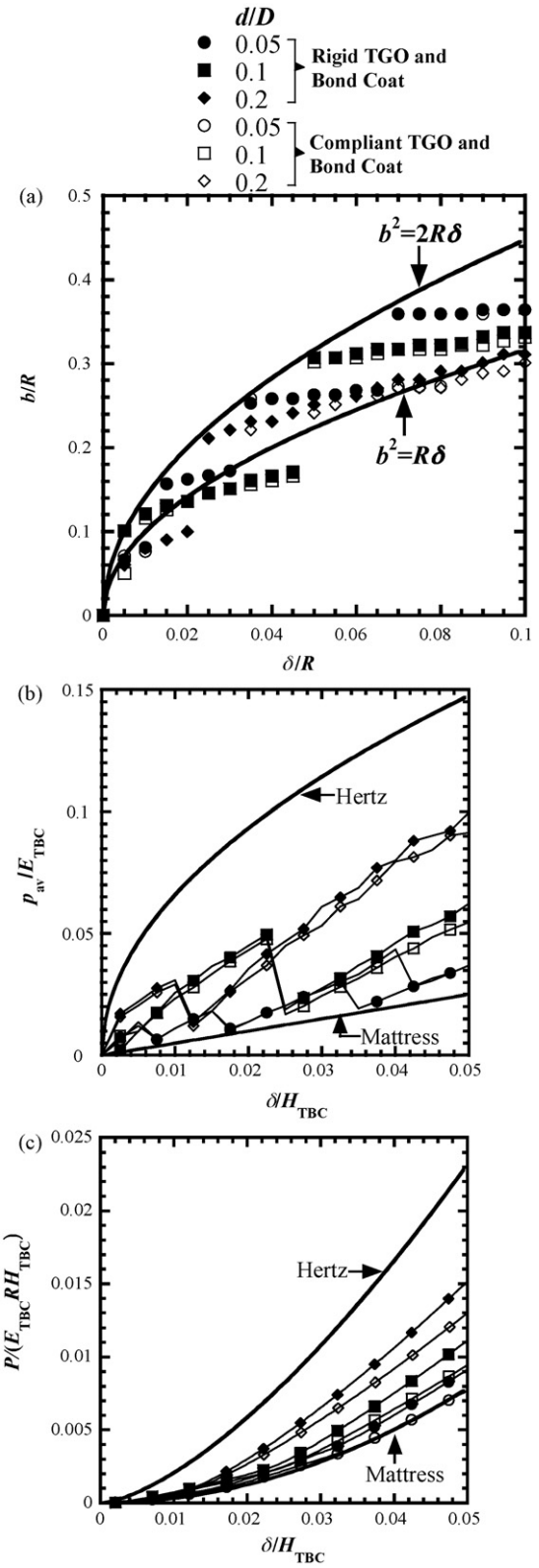

Fig. 7. (a) Contact radius (b) average pressure and (c) indentation load as a function of normalised indentation depth. The effect of the columnar diameter is explored for rigid and compliant TGO/bond coat substrates. $R = 100\,\mu m$, $H_{TBC} = 200\,\mu m$, $g = 0.1\,\mu m$, $\mu_c = \mu_s = 0$, $d = 10, 20, 40\,\mu m$.

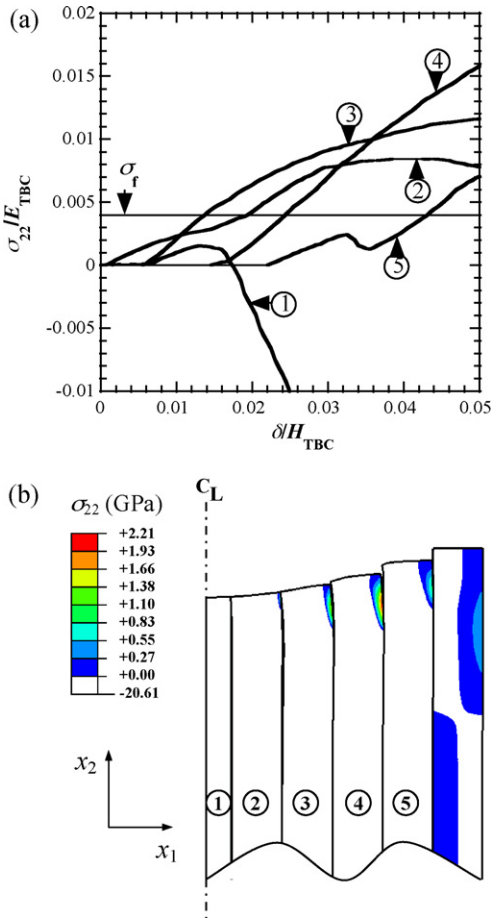

Fig. 8. (a) Normalised tensile axial stress σ_{22}, at the right hand side boundaries of the five first columns from the centre line, as a function of the normalised indentation depth. The critical tensile stress for fracture at the boundaries of the columns to occur is added. (b) Contours of tensile stress σ_{22} near the surface at $\delta/H_{TBC} = 0.05$. $R = 100\,\mu m$, $d = 10\,\mu m$, $g = 0.1\,\mu m$, $H_{TBC} = 200\,\mu m$, $\mu_c = \mu_s = 0$, rigid TGO/bond coat substrate.

surface of the columns and at a depth of approximately $d/2$. With increasing indent depth, the highest stresses are on the order of $0.01–0.015E_{TBC}$, and are attained within the columns labelled 3 and 4, see Fig. 8(a). The level of these stresses is somewhat less than the elasto-dynamic peak value of $0.06E_{TBC}$, but are of sufficient magnitude to cause tensile fracture of the columns. The above predictions for quasi-static, elastic–brittle fracture are in broad agreement with experimental observations of erosive damage; see for example Wellman and Nicholls [12]. In these experimental studies, edge cracking is reported at a depth of $0.5d–2d$.

An order of magnitude estimate can be made for the tensile strength of the TBC layer, as follows. Assume the YSZ columns possess a mode I fracture toughness of $K_C = 1\,MPa\sqrt{m}$ [13], and contain inherent edge flaws of depth 1 μm. (These flaws result from the fern leaf dendritic microstructure at the edge of each column.) Then, the tensile strength equals approximately 560 MPa $\approx 0.004E_{TBC}$. It is evident from Fig. 8(a) that this tensile strength is exceeded first in the 3rd column at $\delta/H_{TBC} = 0.015$, and subsequently in columns 2, 4 and 5.

In additional simulations (not reported explicitly here for the sake of brevity), the level of peak axial stress within each column was explored for $0 < \mu_c < 5$, $0 < \mu_s < 5$, and $0.001 < g/d < 0.1$. Only a moderate effect of friction coefficients and gap width upon stress level was noted: for any given value of indent depth, the maximum value of σ_{22}/E_{TBC} varies by less than a factor of 2 over the parameter range. The response is sensitive, however, to the column diameter d,

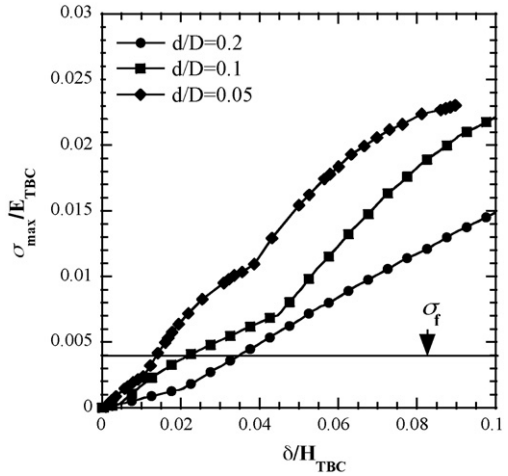

Fig. 9. (a) Normalised spatial maximum tensile stresses, at the right hand side boundaries of the five first columns from the centre line, as a function of the normalised indentation depth. Results are shown for $d = 10$, 20 and 40 μm. The anticipated fracture stress σ_f is included. $R = 100$ μm, $g = 0.1$ μm, $H_{TBC} = 200$ μm, $\mu_c = \mu_s = 0$, rigid TGO/bond coat substrate.

see Fig. 9. Results are shown for $0.05 < d/D < 0.2$ ($R = 100$ μm, $d = 10$, 20, 40 μm), and it is clear that the smaller the column diameter, the higher is the tensile stress with the TBC coating.

5. Finite element predictions of the elastic–plastic indentation response

Finite element simulations are now reported for frictionless spherical indentation of an elastic, ideally plastic columnar TBC. An extensive literature already exists on the quasi-static elastic–plastic indentation of homogeneous layers and thin coatings [14–16]. But TBCs cannot be considered as homogeneous and isotropic layers: the microstructure is anisotropic due to the frictional gaps between columns, and the impression depths are sufficiently large for the measurements to be affected by the properties of the underlying substrate.

The finite element model used for elastic–plastic indentation was similar to that described in Section 3.2 for elastic indentation, but in this case we allowed the columnar TBC layer and the underlying TGO/bond coat to yield. Elastic, ideally plastic behaviour was assumed for each layer, with yield in accordance with the usual von Mises flow theory of plasticity. In this initial scoping study, each layer was taken to be either elastic or elastic, ideally plastic with a yield strength as catalogued in Table 2. The sensitivity of the plastic response to various material and geometric parameters is explored; these included the columnar diameter, gap width, layer height of the TBC and the intercolumnar Coulomb friction coefficient μ_c.

5.1. Effect of gap width upon the elastic–plastic indentation response

The dimensionless contact radius b/R, average pressure p_{av}/σ_{TBC} and the indentation load, $P/R^2\sigma_{TBC}$ are each plotted in Fig. 10 as a function of the dimensionless indentation depth δ/R for selected values of gap width $g = 0.01$, 0.1 and 1 μm. The TBC rested upon either a rigid substrate or upon elastic, ideally plastic layers of TGO and bond coat. All contacts were assumed frictionless. The TBC layer was of height $H_{TBC} = 200$ μm, and comprised columns of diameter 10 μm. The radius of the indenter was $R = 100$ μm.

The dependence of the contact radius b upon the indent depth δ is now shown in Fig. 10(a). As the dimensionless indentation depth δ/R increases, the contact proceeds from one column to the next and

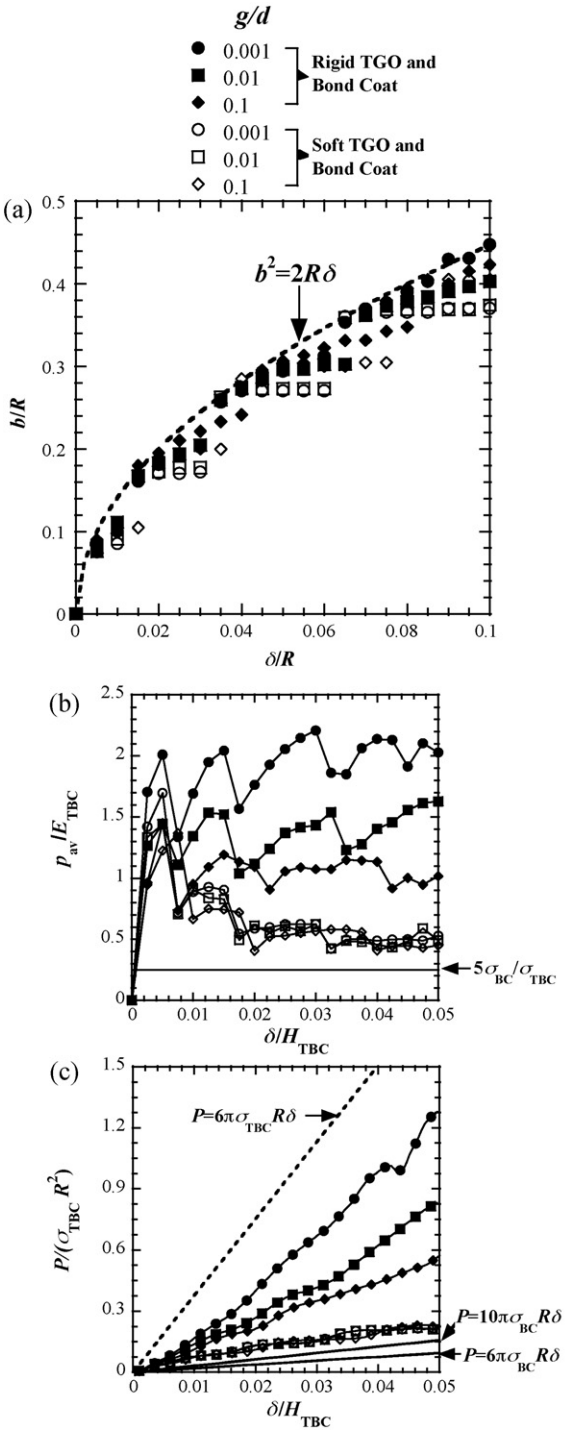

Fig. 10. (a) Contact radius (b) average pressure and (c) indentation load as a function of normalised indentation depth. The effect of the gap width is explored for elastic, ideally plastic TGO and bond coat layers, and for a rigid TGO/bond coat substrate. $R = 100$ μm, $H_{TBC} = 200$ μm, $d = 10$ μm, $\mu_c = \mu_s = 0$.

a step-wise increase in the contact radius b/R is observed. The gap width has a minor effect upon the dimensionless contact radius regardless of whether the TGO/bond coat substrate was elastic-ideally plastic or rigid. The contact radius is adequately represented by $b^2 = 2R\delta$.

The dimensionless average pressure and indentation load are plotted as a function of dimensionless indentation depth δ/H_{TBC} in Fig. 10(b) and (c), respectively. For reference purposes, recall that for the homogeneous half-space the constraint factor is

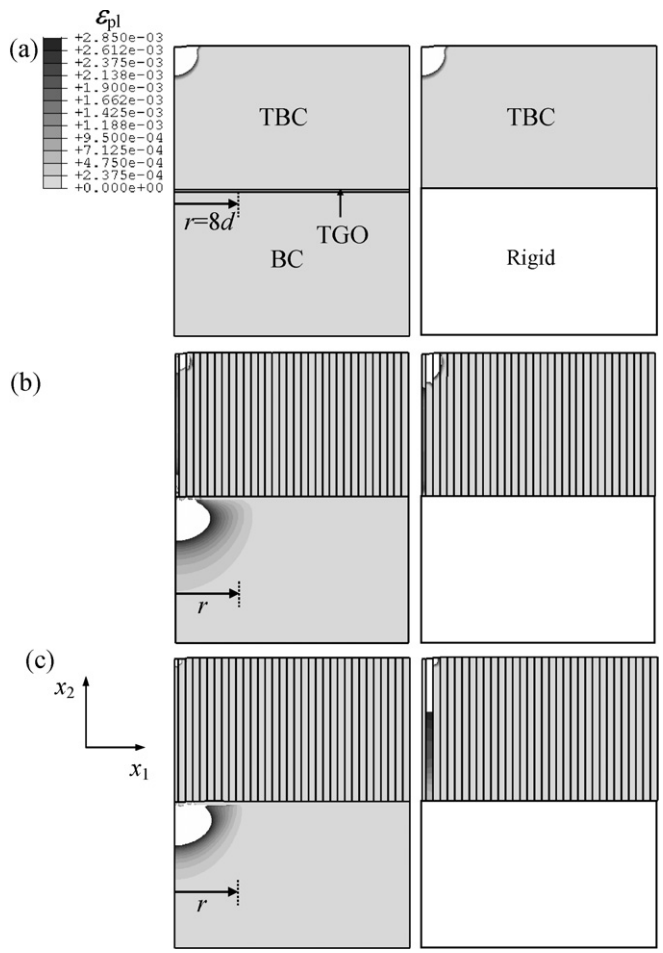

Fig. 11. Contours of equivalent plastic strain at $\delta/H_{TBC} = 0.01$ for (a) homogeneous TBC layer, (b) TBC with $g/d = 0.001$ and $\mu_c = 5$ and (c) TBC with $g/d = 0.1$ and $\mu_c = 0$ for elastic, ideally plastic TGO and bond coat layers, and for a rigid TGO/bond coat substrate. The white color indicates $\varepsilon_{pl} > \varepsilon_{TBC}$ ($R = 100$ μm, $d = 10$ μm, $H_{TBC} = 200$ μm, $\mu_s = 0$).

$C \equiv p_{av}/\sigma_{TBC} = 3$ and is independent of the indentation depth, δ/H_{TBC}. The curves are not smooth due to the discrete nature of the transfer of contact from column to column. The constraint factor C fluctuates with increasing δ/H_{TBC} about a steady mean value. For the case of a rigid TGO/bond coat substrate, this mean value increases somewhat from 1 to 2 with decreasing gap width g. In contrast, when the TGO and bond coat system was allowed to deform in an elastic-ideally plastic manner, the gap width exhibits a minor role and the average indentation pressure p_{av} is of order five times the yield strength σ_{BC} of the bond coat, $p_{av} \approx 5\sigma_{BC}$.

Contours of equivalent plastic strain at an indent depth of $\delta/H_{TBC} = 0.01$ are shown in Fig. 11. Plots are given in Fig. 11(a) for a homogeneous TBC layer of properties given in Table 2 but without intercolumnar gaps, in Fig. 11(b) for a columnar layer with $g/d = 0.001$ and $\mu_c = 5$, and in Fig. 11(c) for a columnar layer with $g/d = 0.1$ and $\mu_c = 0$. The left hand set of plots are for the TBC layer resting on an elastic, ideally plastic substrate, whereas the right hand set of plots are for the TBC layer on a rigid substrate. When the TBC layer is treated as a homogeneous continuum (Fig. 11(a)), the plastic indentation zone is superficial and does not extend to the bottom of the TBC layer. Consequently, the nature of the substrate has a negligible effect upon the indentation response. In contrast, the indentation response is sensitive to the yield strength of the TGO/bond coat substrate when the TBC layer is columnar, see Fig. 11(b) and (c). When the TGO and bond coat layers are taken to be elastic, ideally plastic, the indenter pushes the contacting columns of the TBC layer down into the TGO/bond coat. The degree of indentation of the underlying substrate was larger when the intercolumnar gaps are large and the level of intercolumnar friction is low; compare Fig. 11(b) and (c).

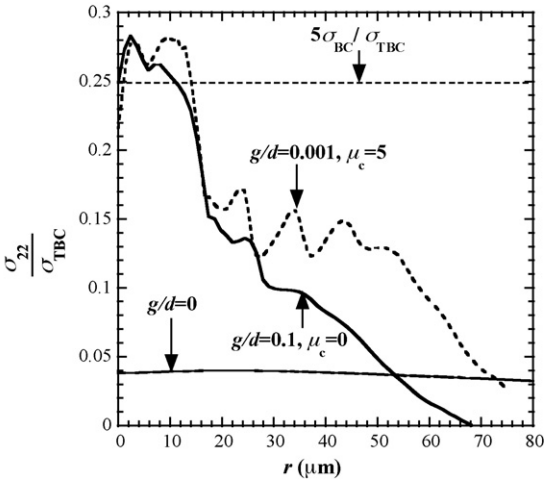

Fig. 12. Radial distribution of tensile axial stress σ_{22} at the TGO/bond coat interface for the choices: $g = 1$ μm and $\mu_c = 0$; $g = 0.01$ μm and $\mu_c = 5$ and for a homogeneous TBC layer at indentation depth $\delta/H_{TBC} = 0.01$. In all cases, $R = 100$ μm, $H_{TBC} = 200$ μm, and $\mu_s = 0$).

Additional insight is obtained by plotting the radial distribution of compressive normal traction along the TGO/bond coat interface in Fig. 12. Results are shown for an elastic, ideally plastic TGO layer and bond coat layer (with the properties specified in Table 2). The same three cases as shown in Fig. 11 are re-considered here: (a) homogeneous TBC layer, (b) $g/d = 0.001$ with $\mu_c = 5$ and (c) $g/d = 0.1$ with $\mu_c = 0$. As already noted, for the case of a columnar TBC layer the compressive stress σ_{22} reaches a value of about $5\sigma_{BC}$ over a central circular patch of radius $1.5d$. This pressure is of the order of the cavitation pressure for the bond coat and is elevated above the indentation pressure for the bond coat of $3\sigma_{BC}$ due to the constraint of the TGO and TBC layer. A negligible transfer of load occurs from one TBC column to the next, and so the axial loads within the TBC columns are borne by the underlying soft bond coat. It is emphasised that this argument only holds when the TBC columns are perfectly aligned and parallel. In reality, the columns grow competitively by epitaxial deposition onto the polycrystalline TGO. They interlock each other and at the bottom of the TBC they resemble a fully polycrystalline ceramic. Consequently, the load carried by the top of the columns is diffused somewhat at the bottom of the TBC. Consequently, yield of the bond coat is obviated. This is consistent with the experimental evidence that erosion of the TBC layer rarely leads to plastic indentation of the underlying bond coat. When full interlock of the columnar microstructure occurs, the TBC layer acts as a homogeneous, isotropic continuum and the level of compressive normal stress on the TGO/bond coat interface is negligible, see the curve labelled $g/d = 0$ in Fig. 12.

5.2. *Effect of intercolumnar friction upon the elastic–plastic indentation response*

Fig. 13 shows the sensitivity of the indentation response to the Coulomb friction coefficient μ_c between the columns. Results are shown for the gap widths $g = 0.1$ and 0.01 μm. The height of the layer was held fixed at $H_{TBC} = 200$ μm, the radius of the indenter was $R = 100$ μm and the contact between the sphere and the columnar layer was considered frictionless. Again, results are shown for an elastic, ideally plastic TGO and bond coat, and also for the TBC layer adhered to a rigid substrate.

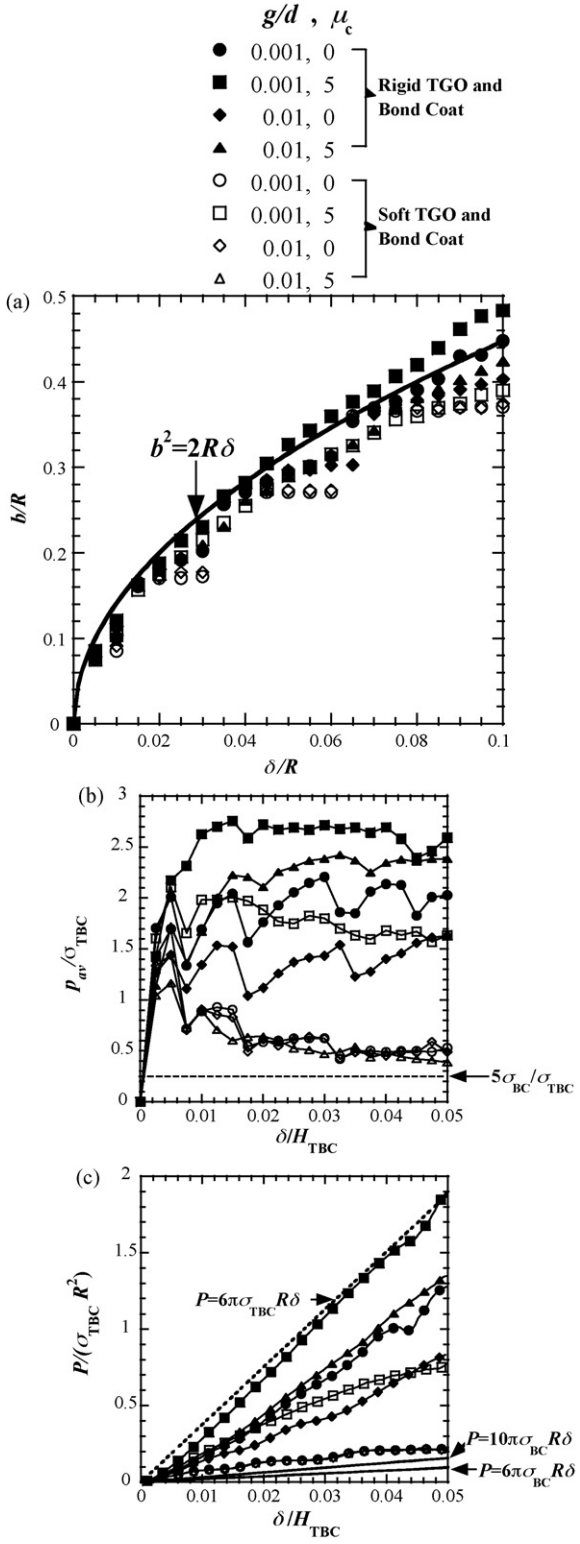

Fig. 13. (a) Contact radius, (b) average pressure and (c) indentation load, as a function of normalised indentation depth. The effect of the intercolumnar friction μ_c is explored for $g = 0.1$ μm and $g = 0.01$ μm, for elastic, ideally plastic TGO and bond coat layers, and for a rigid TGO/bond coat substrate. In all cases, $R = 100$ μm, $H_{TBC} = 200$ μm, $d = 10$ μm, $\mu_s = 0$.

The dimensionless contact radius b/R is plotted in Fig. 13(a) as a function of the dimensionless indentation depth δ/R. We conclude that the intercolumnar Coulomb friction coefficient μ_c has a minor effect upon the dimensionless contact radius b/R, and the contact radius increases slightly upon making the substrate rigid. Pile-up at the contact periphery is negligible, and the simple geometric relation $b^2 = 2R\delta$ suffices.

Fig. 13(b) and (c) presents the effect of the intercolumnar friction coefficient upon the dimensionless average pressure and indentation load, respectively. Consider first the case of a rigid underlying substrate of TGO/bond coat. The constraint factor $C \equiv p_{av}/\sigma_Y$ increases from 1 to 3 with decreasing gap width g and increasing intercolumnar friction coefficient. The indentation load is adequately predicted by Eq. (17) provided the sensitivity of C to

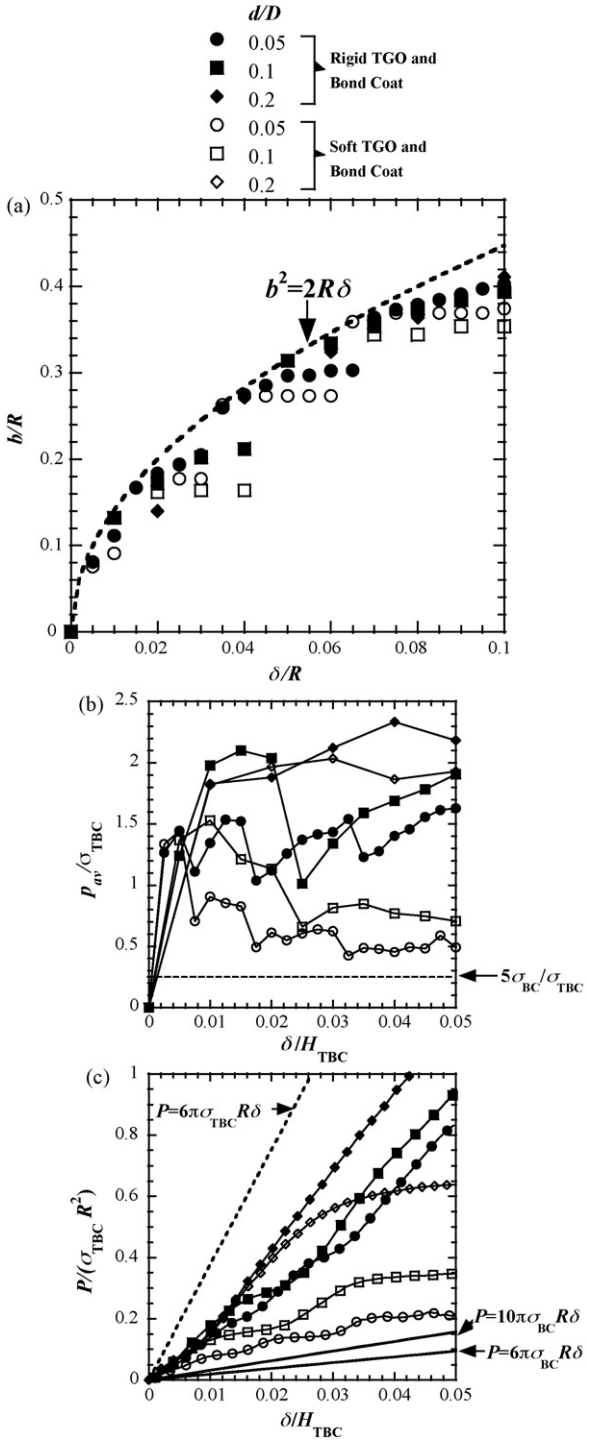

Fig. 14. (a) Contact radius (b) average pressure and (c) indentation load, as a function of normalised indentation depth. The effect of the column diameter is explored for elastic, ideally plastic TGO and bond coat layers, and for a rigid TGO/bond coat substrate ($R = 100$ μm, $H_{TBC} = 200$ μm, $g = 0.1$ μm, $\mu_c = \mu_s = 0$, $d = 10$, 20, 40 μm).

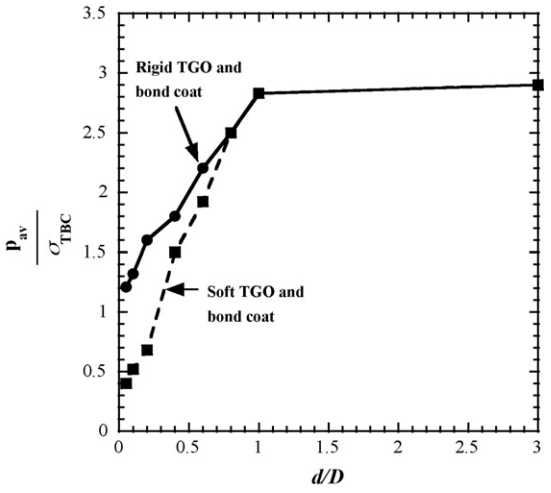

Fig. 15. Constraint factor $C = p_{av}/\sigma_{TBC}$ as a function of d/D for elastic, ideally plastic TGO and bond coat layers, and for a rigid TGO/bond coat substrate. In all cases considered, $R = 100\,\mu m$, $H_{TBC} = 200\,\mu m$, $g = 0.1\,\mu m$ and $\mu_c = \mu_s = 0$.

g and μ_c are taken into account. Second, consider the response of a TBC layer upon an elastic-ideally plastic TGO and bond coat substrate. When the gap width g is large, $g/d > 0.001$, the TBC columns act as independent load-bearing units upon the soft bond coat, and the average indentation pressure is of order $5\sigma_{BC}$, regardless of the level of intercolumnar friction. In contrast, at the small gap width of $g/d = 0.001$, the columns contact each other in the indentation zone and the response is sensitive to the value of μ_c; when the columns are frictionless, the contact pressure is again of order $5\sigma_{BC}$, but at a high value of $\mu_c = 5$, the columns interact and the contact pressure rises to about $1.5\sigma_{TBC}$. Note that the soft bond coat yields in this case and consequently the contact pressure is less than the value of 3 as achieved for the rigid substrate.

5.3. Effect of the columnar diameter upon the elastic–plastic indentation response

Fig. 14 presents the effect of the column diameter d upon the indentation response. The radius of the sphere was held fixed at $R = 100\,\mu m$, the gap width g is $0.1\,\mu m$ and all contacts were assumed frictionless. In order to vary the ratio d/D the diameter of the column was assigned the following values: $d = 10$, 20 and $40\,\mu m$. The height of the TBC layer was $200\,\mu m$ and results are presented for both elastic, ideally plastic TGO/bond coat and for a rigid TGO/bond coat substrate. It is clear from Fig. 14(a) that the dimensionless contact radius b/R is only mildly sensitive to the column diameter and the contact radius b is adequately described by $b^2 = 2R\delta$.

The dimensionless average pressure and indentation load are plotted as a function of the dimensionless indentation depth in Fig. 14(b) and (c), respectively.

For the choice of a rigid substrate the constraint factor increases with increasing columnar diameter. As d/D increases the constraint factor approaches 3, corresponding to the homogeneous substrate. The indentation load is represented by (16), but with a constraint factor C which depends upon d/D, see Fig. 14(c). Now consider the case where the TGO/bond coat substrate is soft. For small columnar diameters the indentation response is dictated by the yield strength of the bond coat, and the average indentation pressure is somewhat above $5\sigma_{BC}$. At a larger column diameter ($d/D = 0.2$), the average indentation pressure increases to about $1.5\sigma_{TBC}$. As the TBC columns diameter increases they function in a manner closer to that of a homogeneous layer than that of an array of independent columns. This is made evident by plotting the constraint factor $p_{av}/\sigma_{TBC} \equiv C$ in terms of d/D for rigid and soft TGO/bond coat substrates, see Fig. 15. The constraint increases with increasing d/D until a saturated value of 3 is attained at $d/D \approx 1$. This limit is the response for a homogeneous TBC layer.

6. Concluding remarks

The above calculations reveal that the details of the elastic and the elastic–plastic indentation response of a columnar thermal barrier coating are sensitive to the ratio of column diameter to diameter of indent, to the gap width and to the level of intercolumnar friction. With diminishing gap width and with increasing level of intercolumnar friction, the indentation pressure increases from that given by the mattress model (elastic or plastic) to that characteristic of a homogeneous half-space.

This study supports the notion that particle erosion of thermal barrier coatings involves the quasi-static indentation of the coating, and the stresses so-generated are sufficient to lead to cracking of the columns near the top surface. The analytical formulae are useful in the generation of an erosion mechanism map, and some steps along this direction are given in the recent study of Evans et al. [6].

References

[1] A.G. Evans, M.Y. He, J.W. Hutchinson, Mechanics-based scaling laws for the durability of thermal barrier coatings, Progress in Material Science 46 (2001) 249–271.
[2] Th. Zisis, N.A. Fleck, Mechanisms of elastodynamic erosion of electron-beam thermal barrier coatings, International Journal of Materials Research 98 (2007) 1196–1202.
[3] X. Chen, J.W. Hutchinson, A.G. Evans, Simulation of the high temperature impression of thermal barrier coatings with columnar microstructure, Acta Materialia 52 (2004) 565–571.
[4] R.G. Wellman, M.J. Deakin, J.R. Nicholls, The effect of TBC morphology on the erosion rate of EB PVD TBCs, Wear 258 (2005) 349–356.
[5] M. Watanabe, C. Mercer, C.G. Levi, A.G. Evans, A probe for the high temperature deformation of thermal barrier oxides, Acta Materialia 52 (2004) 1479–1487.
[6] A.G. Evans, N.A. Fleck, S. Faulhaber, N. Vermaak, M. Maloney, R. Darolia, Scaling laws governing the erosion and impact resistance of thermal barrier coatings, Wear 260 (2006) 886–894.
[7] K.L. Johnson, Contact Mechanics, Cambridge University Press, 1985.
[8] H.J. Frost, M.F. Ashby, Deformation Mechanism Maps, Pergamon Press, 1982.
[9] A.F. Bower, N.A. Fleck, A. Needleman, N. Ogbonna, Indentation of a power law creeping solid, Proceedings of the Royal Society 441 (1993) 97–124.
[10] M. Watanabe, T. Xu, A.S. Gandhi, C.G. Levi, A.G. Evans, Shear band formation in columnar thermal barrier oxides, Acta Materialia 53 (2005) 3765–3773.
[11] ABAQUS version 6. 2 User's Manual Hibbitt, Karlsson and Sorensen Inc., Pawtucket, RI, 2001.
[12] R.G. Wellman, J.R. Nicholls, Some observations on erosion mechanisms of EB PVD TBCs, Wear 242 (2000) 89–96.
[13] A.G. Evans, D.R. Mumm, J.W. Hutchinson, G.H. Meier, F.S. Pettit, Mechanisms controlling the durability of thermal barrier coatings, Progress in Material Science 46 (2001) 505–553.
[14] T.Y. Tsui, J. Vlassak, W.D. Nix, Indentation plastic displacement field. Part I. The case of soft films on hard substrates, Journal of Materials Research 14 (6) (1999) 2204–2209.
[15] T.Y. Tsui, J.J. Vlassak, W.D. Nix, Indentation plastic displacement field. Part II. The case of hard films on soft substrates, Journal of Materials Research 14 (6) (1999) 2196–2203.
[16] X. Chen, J. Vlassak, A numerical study on the measurement of thin film mechanical properties by means of nanoindentation, Journal of Materials Research 16 (2001) 2974–2982.